Check for updates

View Article Online
View Journal

PCCP
Physical Chemistry Chemical Physics

Accepted Manuscript

This article can be cited before page numbers have been issued, to do this please use: D. L. Z. Caetano, R. Metzler, A. G. Cherstvy and S. J. de Carvalho, *Phys. Chem. Chem. Phys.*, 2021, DOI: 10.1039/D1CP03185F.

This is an Accepted Manuscript, which has been through the Royal Society of Chemistry peer review process and has been accepted for publication.

Accepted Manuscripts are published online shortly after acceptance, before technical editing, formatting and proof reading. Using this free service, authors can make their results available to the community, in citable form, before we publish the edited article. We will replace this Accepted Manuscript with the edited and formatted Advance Article as soon as it is available.

You can find more information about Accepted Manuscripts in the Information for Authors.

Please note that technical editing may introduce minor changes to the text and/or graphics, which may alter content. The journal's standard Terms & Conditions and the Ethical guidelines still apply. In no event shall the Royal Society of Chemistry be held responsible for any errors or omissions in this Accepted Manuscript or any consequences arising from the use of any information it contains.

View Article Online
DOI: 10.1039/D1CP03185F

PCCP

ARTICLE TYPE

Cite this: DOI: 00.0000/xxxxxxxxxx

Adsorption of Lysozyme Into a Charged Confining Pore†

Daniel L. Z. Caetano,[ab] Ralf Metzler,[c] Andrey G. Cherstvy,[cd] and Sidney J. de Carvalho[e]

Received Date
Accepted Date

DOI: 00.0000/xxxxxxxxxx

Several applications arise from the confinement of proteins on surfaces since their stability and biological activity are enhanced. It is also known that the way a protein adsorbs on the surface is important for its biological function since its active sites should not be obstructed. In this study, the adsorption properties of hen egg-white Lysozyme, HEWL, into a negatively charged silica pore is examined employing a coarse-grained model and constant–pH Monte Carlo simulations. The role of electrostatic interactions is taken into account when including the Debye-Hückel potentials into the Cα structure-based model. We evaluate the effects of pH, salt concentration, and pore radius on the protein preferential orientation and spatial distribution of its residues regarding the pore surface. By mapping the residues that stay closer to the pore surface, we find the increase of pH leads to orientational changes of the adsorbed protein when the solution pH gets closer to the HEWL isoelectric point. At these conditions, the pK_a shift of these important residues caused by the adsorption into the charged confining surface results in a HEWL charge distribution that stabilizes the adsorption in the observed protein orientation. We compare our observations to the results of pK_a shift for HEWL available in the literature and to some experimental data.

1 Introduction

The adsorption of proteins on confining surfaces, as routinely taking place in porous materials, has attracted considerable attention in recent years[1,2]. This interest is due mainly to the broad applicability in biosensors, biocatalysts, and biomolecule delivery systems development[3–6]. In these cases, the conditions of confinement lead to the protection of proteins against denaturation conditions and biological degradation, enhance their chemical and thermal stability, and, therefore, increase their biological activity. The study of native structure stability of proteins in nanopores has also provided relevant results for understanding the physical basis of protein folding[7–9]. Furthermore, confined biomolecules are also used as models to study the biological transportation in biomembrane pores[10,11].

One of the determining factors for the applicability of confined proteins is their orientation regarding the surface and the consequent exposure of their active sites. The confinement effects on their native structure and the properties related to biological function, such as the local charge distribution, should be reduced[14]. Experiments show that encapsulated proteins on charged surfaces exhibit an enhanced activity as compared to hydrophobic surfaces where this increase is highly dependent on the size and geometry of the cavity[15–17]. In general, maximum adsorption is observed when the pH is close to the isoelectric point of the protein, and this trend is understood in purely electrostatic (ES) terms. At these conditions, the protein–protein repulsive interactions are minimal and the process is governed predominantly by the attractive protein–surface interactions[18–21].

Several computational studies have addressed the interactions between proteins and charged surfaces[22,23]. Atomistic models were used to identify the preferential orientation and the most important residues for the adsorption. These studies focused, for instance, on Lysozyme and α-Chymotrypsin adsorption onto silica surfaces[24,25]; Lysozyme, Cytochrome C, and Ribonuclease A adsorption onto self-assembled monolayers[26–28]; and β-Lactoglobulin adsorption onto solid Au surfaces[29]. Coarse-grained models have been adopted to investigate the salt and pH effects[30–35]. An important aspect is the effect of surface ES potential on the degree of protonation of protein residues, the so-called charge regulation[36–39]. In this case, a significant contribution to

[a] Institute of Chemistry, State University of Campinas (UNICAMP), Campinas, Brazil.
[b] Center for Computational Engineering and Sciences, State University of Campinas (UNICAMP), Campinas, Brazil.
[c] Institute for Physics & Astronomy, University of Potsdam, 14476 Potsdam-Golm, Germany.
[d] Institut für Physik, Humboldt-Universität zu Berlin, 12489 Berlin, Germany.
[e] Department of Physics, São Paulo State University (UNESP), Institute of Biosciences, Humanities and Exact Sciences, São José do Rio Preto, Brazil. E-mail:sidney.carvalho@unesp.br

† Electronic Supplementary Information (ESI) available: Fig. S1 contains the fraction of contacts, mean radius of gyration, root-mean-square deviation, and mean binding energy of a single HEWL protein into a negatively charged pore, as a function of the pore radius, for pH = 7, 9, and 11 at a salt concentration of 0.001 M. Fig. S2 contains the fluctuations of binding energy, net charge, and fluctuations of net charge of a single HEWL protein into a negatively charged pore, as a function of pH, for pore radius $a = 40$, 80, 120, and 160 Å at a salt concentration of 0.001 M. Tables S1 and S2 show the Hill coefficient for all HEWL's basic residues at low (0.001 M) and high (0.2 M) salt concentrations. See DOI: 00.0000/00000000.

Published on 05 November 2021. Downloaded by Technical University of Munich on 11/5/2021 7:35:48 PM.

Physical Chemistry Chemical Physics Accepted Manuscript

View Article Online
DOI: 10.1039/D1CP03185F

Published on 05 November 2021. Downloaded by Technical University of Munich on 11/5/2021 7:35:48 PM.

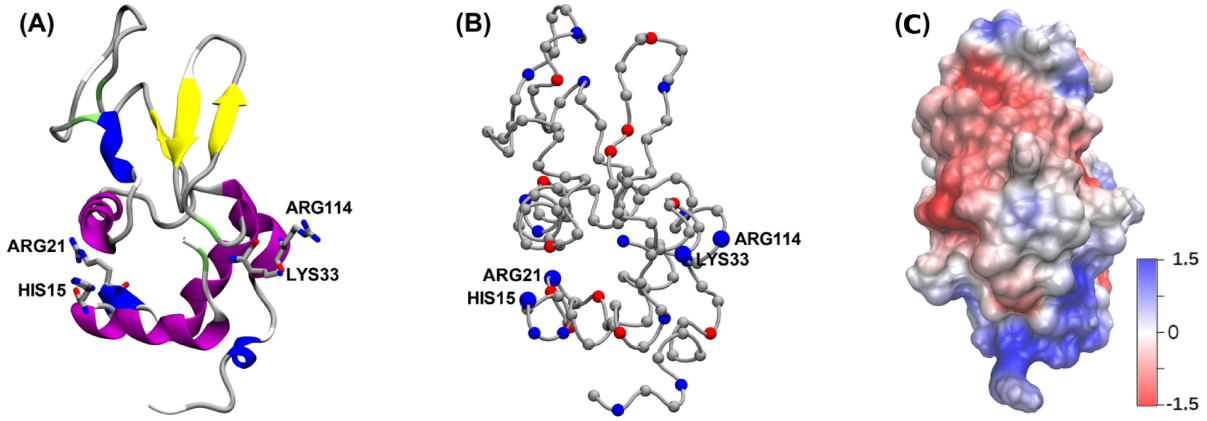

Fig. 1 (A) Structure of hen egg-white Lysozyme (HEWL) protein built from PDB-ID 3WUN. The side chains of four important residues for HEWL–surface adsorption and orientation are shown. (B) Cα representation of HEWL, where the basic residues (arginine, lysine, and histidine) are highlighted in blue, and the acidic ones (tyrosine, aspartic, and glutamic acids) are highlighted in red. (C) ES potential at the HEWL surface calculated using APBS Electrostatic Extension of VMD [12,13] considering the mean charges obtained from our simulation in the solution at the isoelectric point and salt concentration of 100 mM. The negative potentials are shown in red, while the positive ones are in blue. The unit of electrostatic potential is k_BT/e ($\approx$ 25 mV)

.

the binding free energy is observed at pH close to the isoelectric point of the protein and it is not noticed by constant–charge models [39–41]. Despite of these efforts, molecular simulations of protein adsorption on charged confining surfaces are still scarce. [42,43].

In the current paper, we study the adsorption properties of hen egg-white Lysozyme (HEWL) into a negatively charged pore employing constant–pH Monte Carlo simulations. This protein is usually adopted as a model system to study protein adsorption onto porous materials [44]. One of its functions is, for instance, the hydrolysis of the cell walls of Gram-positive bacteria [45,46]. We adopt a coarse-grained model in which the ES interaction between the protein's charged residues and between them and the surface is given by the Debye-Hückel potentials [47,48]. The charges of titratable residues are affected not only by the solution conditions (salt concentration and pH), but also by the presence of the vicinal charged surface. We evaluate the influence of pH, salt concentration, and confinement radius on the protein–pore interactions and the distribution of charged residues relative to the pore surface. The effect of the confining–surface ES potential on the protonation degree of the residues is also analyzed, and its importance to the adsorption features is discussed.

The paper is organized as follows: in Sec. 2 we present the protein model employed and the details of our computer simulations. In Sec. 3 we examine the influence of salt concentration, pH, and confinement radius on protein–pore interactions and discuss the main findings. Finally, we conclude and outline some possible applications of our results in Sec. 4.

2 Model and Simulations

HEWL, see Fig. 1, is a small ellipsoidal enzyme constituted by a single chain with 129 amino-acid residues. Among its 129 residues, seven are aspartic acids (ASP), two are glutamic acids (GLU), three are tyrosines (TYR), one histidine (HIS), six are lysines (LYS), and eleven are arginines (ARG). The distribution of the residues results in an isoelectric point of about 11 [24]. We model this protein according to the structure-based model (SBM), in which its residues are represented by single spheres centered at the Cα position [49–54], and the non–ES energy is given by

$$\begin{aligned} V(r,\theta,\phi) \;=\; & \sum_{\text{bonds}} \varepsilon_r (r-r_0)^2 + \sum_{\text{angles}} \varepsilon_\theta (\theta-\theta_0)^2 + \\ & \sum_{\text{dihedrals}} \varepsilon_\phi \left\{ [1-\cos(\phi-\phi_0)] + \frac{1}{2}[1-\cos(3(\phi-\phi_0))] \right\} + \\ & \sum_{\text{contacts}} \varepsilon_c \left[5\left(\frac{d_{ij}}{r_{ij}}\right)^{12} - 6\left(\frac{d_{ij}}{r_{ij}}\right)^{10} \right] + \\ & \sum_{\text{non-contacts}} \varepsilon_{nc} \left(\frac{\sigma_{nc}}{r_{ij}}\right)^{12}, \end{aligned} \tag{1}$$

where r, θ, and ϕ are the distances between two consecutive residues, the angles formed by three consecutive residues, and the dihedral angles formed by four consecutive residues, respectively. The values of r_0, θ_0, and ϕ_0 are obtained from the native structure of HEWL (PDB-ID 3WUN). The parameter d_{ij} is the distance between residues i and j ($i < j-3$) that are in contact in the native structure, according to the CSU (Contact of Structural Units) contact map [55]. The parameters $\varepsilon_r = 100\varepsilon_c$, $\varepsilon_\theta = 20\varepsilon_c$ and $\varepsilon_\phi = \varepsilon_{nc} = \varepsilon_c$ are defined as a function of the Lennard-Jones $10-12$ parameter ε_c. It determines the interaction energy between the residues in contact in the native structure and, accordingly, the transition temperature to the unfolded state. To set the value of ε_c, we associate the unfolding–transition temperature obtained from the simulations, usually obtained from the peak of heat capacity, C_v [54], with the melting temperature, T_m, obtained experimentally. We calculate the heat capacities $C_v = (\langle E^2\rangle - \langle E\rangle^2)/k_BT^2$ through the Weighted Histogram Analysis Method (WHAM), which calculates the density of states of the system at a given temperature T, using the energy histograms obatined from simulations at different constant temperatures. [56,57]. Fig. 2 shows C_v calculated from

Physical Chemistry Chemical Physics Accepted Manuscript

View Article Online
DOI: 10.1039/D1CP03185F

Published on 05 November 2021. Downloaded by Technical University of Munich on 11/5/2021 7:35:48 PM.

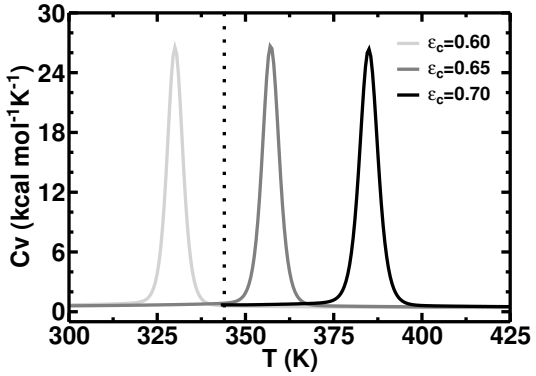

Fig. 2 Heat capacities at constant volume, C_v, in pH = 7.0 and salt concentration of 0.1 M for three different values of ε_c: 0.60 kcal/mol (light gray line), 0.65 kcal/mol (gray line), and 0.70 kcal/mol (black line). We consider that the peak of C_v as the melting temperature, T_m. The vertical dotted line corresponds to the T_m obtained experimentally in Ref. [58] .

simulations for three different values of ε_c, as well as T_m provided in Ref. [58]. Therefore, in this study, we define $\varepsilon_c = 0.63$ kcal/mol to reproduce the melting temperature obtained experimentally. Finally, the parameter regarding the repulsive interactions between residues that do not belong to the native contact map is $\sigma_{nc} = 4.0$ Å [49,50].

The ES interaction energy between any pair of charged residues is given by the screened Coulomb potential

$$V_{res}^{ES}(r_{ij}) = \frac{z_i z_j e_0^2}{4\pi\varepsilon_0\varepsilon_s}\frac{e^{-\kappa r_{ij}}}{r_{ij}}, \qquad (2)$$

where e_0 is the elementary charge, z_i and z_j are the respective valencies of residues i and j, r_{ij} is the distance between them, ε_0 is the permittivity of free space, $\varepsilon_s = 78.7$ is the solvent dielectric constant, and κ^{-1} is the Debye screening length. This model has been successfully used to study the pH-dependent effects for protein folding and stability [47,48,54].

One single protein is confined within a cylindrical charged pore of radius a and surface charge density σ_e, which is a function of pH of the solution. We obtain the values of σ_e for the pH values adopted in this work from the experimental data for the silica nanoparticles presented in Ref. [59], as can be seen in Table 1. The ES interaction energy between the charged residue i of HEWL inside the pore and the charged surface is obtained from the solution of the linear Poisson-Boltzmann equation given by [60,61]

$$V_{pore}^{ES}(r_i) = \frac{2z_i e\sigma_e \mathrm{K}_0(\kappa a)}{\varepsilon_0\varepsilon_s\kappa[\mathrm{K}_0(\kappa a)\mathrm{I}_1(\kappa a)+\mathrm{K}_1(\kappa a)\mathrm{I}_0(\kappa a)]}\mathrm{I}_0(\kappa r_i), \qquad (3)$$

where r_i is the radial distance between the residue i and the pore axis, and I_n and K_n are the modified Bessel functions of first and second kind, respectively. The Debye screening length is given by [62]

$$\kappa^{-1} = \left[\frac{\varepsilon_0\varepsilon_s k_B T}{e^2(2n_0 + n_{ci})}\right]^{1/2}, \qquad (4)$$

where $k_B T$ is the thermal energy, n_0 is the number density of salt ions in the bulk of the solution, and $n_{ci} = (\sigma_e 2\pi a)/(e\pi a^2)$ is the number density of the counterions to keep the system electroneutral.

Table 1 Surface charge density, σ_e, for the pH values adopted in this work, which were obtained from the experimental data for the silica nanoparticles presented in Ref. [59]

pH	σ_e (C/m^2)	pH	σ_e (C/m^2)	pH	σ_e (C/m^2)
3	-0.0005	6	-0.0280	9	-0.1300
4	-0.0055	7	-0.0500	10	-0.1700
5	-0.0140	8	-0.0800	11	-0.2100

To sample protein configurations, we carry out Metropolis Monte Carlo simulations in the canonical ensemble and used five kinds of movements: (1) translational displacement of a single residue randomly chosen, (2) radial displacement of the whole protein, (3) pivot rotation, (4) rotation of the whole protein, and (5) crankshaft movement [63]. In each Monte Carlo step, we randomly choose one of these movements. To sample the protonation state of the residues, we also randomly choose 30% of configurations to try to change the protonation state of titratable residues. In these configurations, we randomly choose a titratable residue, and its protonation state is changed or not according to Metropolis criterion with the energy variation given by [47,48,64]

$$\Delta V^{tit} = \Delta V^{ES} \pm \chi\left[k_B T(\mathrm{pH} - \mathrm{pK}_a^0)\ln 10\right], \qquad (5)$$

where $\chi = 1$ or -1 if the selected residue is basic or acidic, respectively. The positive and negative signs in Eq. (5) are used for protonation and deprotonation, respectively. The first term in Eq. (5) corresponds to the ES energy variation (Eqs. (2) and (3)) in the protonation/deprotonation. The second one is the compound model contribution, where the pK_a^0 is the negative of the logarithm of the dissociation constant in the absence of electrostatic interactions with the other charged residues of the protein. The pK_a^0 value of the titratable residues are 4.0 for aspartic acid, 4.5 for glutamic acid, 9.6 for tyrosine, 6.3 for histidine, 10.6 for lysine, and 12.0 for arginine [48,65]. The cysteine is a titratable residue in its free form. HEWL has eight cysteine residues, but they form four disulfide bonds and cannot ionize. Therefore, in this work, they are considered to be neutral residues [66]. With this approach, we assume any changes in the protonation degree of the ionizable residues are caused by the residue–residue EL interactions. The effects due to detailed residues charge distribution are not taking into account, as well as the desolvation ones, since we do not consider differences between the dielectric constant of the solvent and protein. For a broad description of the different approaches adopted in protonation equilibrium simulations in protein, see Ref [67].

More realistic approaches to constant-pH simulations have been proposed and consider explicit ions in a system coupled to a proton bath whose chemical potential establishes a constant pH. The number of these charged particles fluctuates with the variation of the charge of the protein ionizable residues, obeying the grand-canonical ensemble statistics [69,70]. Some methods also take into account solvent dissociation in simplified water models [71]. In the simplified approach adopted here, the ions are treated implicitly at the mean-field level, and the pH is an input parameter in

Physical Chemistry Chemical Physics Accepted Manuscript

View Article Online
DOI: 10.1039/D1CP03185F

Published on 05 November 2021. Downloaded by Technical University of Munich on 11/5/2021 7:35:48 PM.

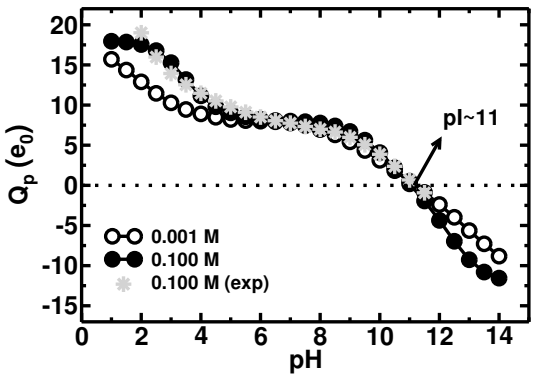

Fig. 3 Net charge, Q_p (in units of elementary charge e_0), of HEWL free in the solution as a function of pH, for salt concentrations of 0.001 (empty black circles) and 0.1 M (filled black circles). The experimental results (light gray stars) were obtained from Ref.[68] .

Eq. (5) that modulates the protonation probability. This allows us to reach a proper sampling of protein ionization states with a relatively short simulation time at any salt concentration[67].

For each combination of pH, salt concentration and pore radius, we start the Monte Carlo simulations with the protein in its native state with all titratable residues charged. Then, the protein configurations are sampled using the movements described above and changing the state of protonation of the titratable residues. The equilibration process was carried out with 10^7 Monte Carlo steps, and the average properties were calculated using 5×10^6 statistically uncorrelated configurations of the protein.

3 Results and Discussions

We start our analysis by evaluating the dependence of the net charge of HEWL free in solution, Q_p, on pH. Fig. 3 shows Q_p obtained from simulations for salt concentrations of 0.001 (empty black circles) and the physiologically relevant salinity 0.1 M (filled black circles) in the absence of confinement. The computational results are in good agreement with the experimental ones (light gray stars) with the isoelectric point (pI ≈ 11)[68] unaffected by variations in the salt concentration C_s. The majority of the pK_a values obtained by simulations present no significant deviation from the experimental ones from Ref.[72] for $C_s = 0.1$ M. For this comparison, we adopt the criterion of Goh and coauthors[73] in which the deviation is considered significant only when the difference regarding the experimental values is higher than a 1.0 pK_a unit. The acidic residues GLU35, ASP66, and ASP87 of HEWL exhibit a deviation of 2.45, 1.36, and 1.43, respectively. Despite its high simplicity, the model adopted in this work is proved suitable to study acid-base equilibrium in proteins[47,48,54].

To verify the conformational stability of the HEWL protein confined in the pore, we carried out simulations in regimes of low (0.001 M) and high (0.1 M) ionic strength and pore radii ranging from 40 to 800 Å (see Fig. S1 in Supplementary Information). The pH range considered was from 7 to 11 since, in these conditions, the protein charge and surface charge density result in stronger ES adsorption. For high salt concentration, the HEWL remains folded with approximately 90% of its native contacts formed (298 out of 330 contacts), a small root-mean-square deviation (RMSD) of about 1.5 Å, and a well-known mean radius of gyration $R_g \approx 14$ Å[74]. In the weak–ES–screening regime corresponding to low salt concentrations, the protein undergoes a conformational transition in which the fraction of native contacts changes from about 0.9 to 0.55 at pore radius $a = 400$ Å. Perturbation on the HEWL secondary structure upon adsorption on silica nanoparticles was also observed in Ref.[75] from deconvolution of circular dichroism spectra.

Based on the analysis above, all of the following results under the conditions in which the protein has some flexibility but retains its native structure ($a < 400$ Å). Fig. 4 shows how pH, salt concentration, and pore radius affect the HEWL–surface binding energy, E_B, that is given by

$$E_B = \left\langle \sum_i V_{pore}^{ES}(r_i) \right\rangle, \tag{6}$$

where the summation is taken over all charged residues, and the average is calculated over the configurations generated by simulation. For both salt concentrations (0.001 M in Fig. 4A and 0.1 M in Fig. 4B), E_B presents a minimum value that becomes deeper and deeper and shifts slightly to higher pH with increasing pore radius. This increase in $|E_B|$ (in other words, it becomes more negative) occurs because the density of positive counterions, n_{ci}, required to neutralize the negative silica surface, and so their contribution to the ES screening depends inversely on the pore radius a (see the definition of n_{ci} in Eq. (4)). The displacement of the pH that corresponds to the strongest binding energy is partially related to the conditions which result in a maximal product between the protein charge and surface charge density and thus in maximal attraction of net-positively charged HEWL and negatively charged silica–surface.

Another factor is the dependence of the directionality degree of the adsorbed protein on the pore radius, as will be seen later. When the binding is very directional, the adsorption is predominantly stabilized by the interaction of the pore surface with the specific positively charged region of the protein. We also see that increasing salt concentration not only decreases $|E_B|$, but also diminishes the pH range in which HEWL is adsorbed. For pH < 6.5, the ES screening variation caused by increase salt concentration from 0.001 to 0.1 M leads from a state in which the protein is strongly adsorbed, and $|E_B|$ is about dozens k_BTs, to a weakly adsorbed state, where $|E_B|$ is about k_BT. Once HEWL's pI is approximately 11 and the silica's point of zero charge is between pH 2 and 4[59], we expected the protein is electrostatically attracted to the pore surface at pH between 2 and 11. However, Fig. 4A shows $E_B < 0$ for pH regimes above this range. $E_B \approx -6 \pm 8\, k_BT$ at pH $= 12$ and low salt concentration, where E_B fluctuations can be seen in Fig. S2A of Supplementary Information. This relatively high fluctuation of E_B is predominantly due to protein charge fluctuations at this pH value, which corresponds to pK_a^0 of arginine residues (see Figs. S2B and S2C in Supplementary Information). This fact suggests charge regulation is the possible driving force for adsorption at pH $\geq$ pI[34,38,39]. A comparison between E_B calculated considering charge regulation and keeping fixed charges can be seen in Fig. 4C for the protein within the pore with radius

Physical Chemistry Chemical Physics Accepted Manuscript

View Article Online
DOI: 10.1039/D1CP03185F

Published on 05 November 2021. Downloaded by Technical University of Munich on 11/5/2021 7:35:48 PM.

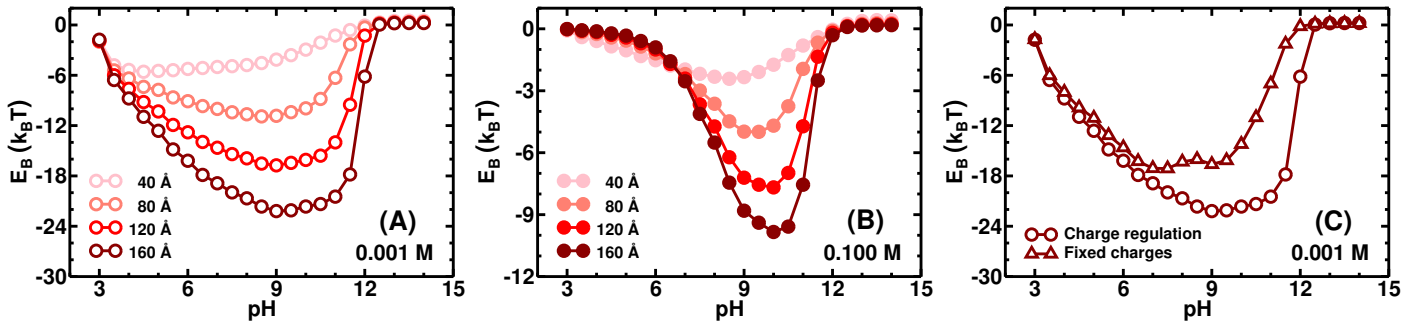

Fig. 4 Mean binding energy, E_B, of a single HEWL protein into a negatively charged pore as a function of pH for two salt concentrations: (A) 0.001 M - empty circles, and (B) 0.1 M - filled circles. The pore radii are $a = 40$ Å (pink circles), 80 Å (light red circles), 120 Å (red circles) and 160 Å (dark red circles). (C) The mean binding energy, E_B, of a single HEWL protein into a negative charge pore of radius $a = 160$ Å and salt concentration of 0.001 M, calculated considering charge regulation (dark red circles) and keeping fixed charges (dark red triangles).

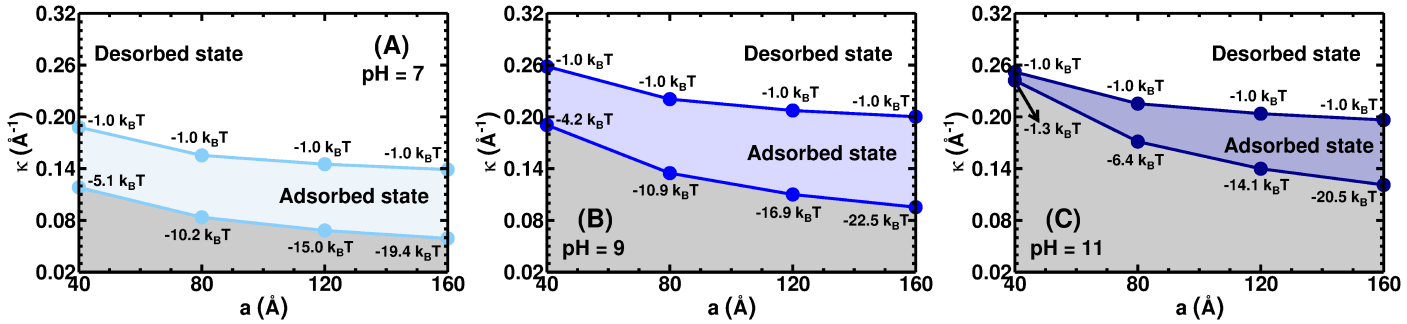

Fig. 5 Pore radius–Debye κ diagram demarking adsorbed and desorbed states of a single HEWL protein into a negatively charged pore for three pHs: (A) pH = 7 (light blue circles), (B) pH = 9 (blue circles), and (C) pH = 11 (dark blue circles). Protein is considered adsorbed when the mean binding energy to the pore surface overcomes the thermal energy ($E_B \leq -k_BT$), which is represented by the line that delimits the upper limit of the regions colored in shades of blue. The line delimiting the regions colored in shades of blue and gray corresponds to the minimum κ value where $n_0 = 0$, that is, there are only counterions in the solution. The values shown in the plots are the mean binding energy, E_B, for each point indicated by the small circles.

$a = 160$ Å at low salt concentration (0.001 M). At pH = 12, the calculations considering fixed charges result in $E_B \approx 0$, in contrast to what was presented above ($E_B \approx -6$ k$_B$T). For pH ranging from approximately 7 to 12, the charge regulation mechanism causes a significant increase in the absolute value of binding energy. The larger difference is observed in pH = 11.5, close to the protein isoelectric point ($\Delta E_B \approx 15$ k$_B$T).

To evaluate the pore radius a and ionic strength effects, Fig. 5 shows a Debye κ–pore radius diagram demarking adsorbed and desorbed states at pH = 7, 9, and 11. As already adopted successfully in Ref.[60] for the inverted adsorption of polyelectrolytes in confinement, the protein is considered adsorbed when the binding energy E_B overcomes the thermal energy ($E_B \leq -k_BT$). The top line separates the adsorbed and desorbed states, whereas the bottom line shows the minimum κ value (see Eq. (4)) that takes into account only the counterions ($n_0 = 0$). Therefore, the electroneutrality is not satisfied in the bottom grey region. The increase of the pore radius, a, results in the decrease of this minimum κ value due to the dependence of the counterions number density, n_{ci}, on a [$n_{ci} = (\sigma_e 2\pi a)/(e\pi a^2)$]. Furthermore, the pH variation from 7 to 11 causes an increase in the minimum κ value due to the larger σ_e (see Table 1). The binding energy values are also shown for each point indicated by small circles of each plot. We can see that at pH = 11, the higher counterions concentration for the smaller pore radius ($a = 40$ Å) almost prevents the adsorption since the minimum κ value corresponds binding energy of -1.3 k$_B$T. For a given Debye length, the ES potential at the pore surface becomes more negative with the increasing pore radius a. Despite that, the κ value needed to cause the protein desorption is smaller for a larger pore radius, suggesting the increase in ES potential does not compensate the increase of entropic penalty caused by the adsorption at a larger pore.

We evaluate the orientation of the adsorbed protein through the probability distribution $\rho(r)$ of charged basic residues as a function of the distance r from the pore surface. Fig. 6 shows $\rho(r)$ of residues HIS15 (yellow line), ARG21 (blue line), LYS33 (dark blue line), ARG61 (dark green line), ARG68 (dark yellow line), and ARG114 (green line) at low salt concentration (0.001 M) and pH = 7, 9, and 11. We focused here on the larger pore ($a = 160$ Å) to minimize the confinement effects. Since the radius of gyration of HEWL remains virtually constant in all cases presented in this study, the residues can be found at specific regions from the pore surface for each pH. Thus, we grouped the charged basic residues into three groups. Group 1 contains all residues that are more likely to locate at $r \leq 10$ Å. Group 2 is composed of the ones that are more likely to find at $10 < r \leq 20$ Å, and the ones that are more likely to locate at $r > 20$ Å belong to Group 3. Table 2 shows the details of all charged basic residues which belong to each group

Physical Chemistry Chemical Physics Accepted Manuscript

View Article Online
DOI: 10.1039/D1CP03185F

Published on 05 November 2021. Downloaded by Technical University of Munich on 11/5/2021 7:35:48 PM.

Table 2 List of basic residues which are more likely located at $r \leq 10$ Å (Group 1), $10\,\text{Å} < r \leq 20\,\text{Å}$ (Group 2), and $r > 20$ Å (Group 3) from the pore surface. The pore radius is $a = 160$ Å and the salt concentration is 0.001 M.

pH	Group 1	Group 2	Group 3
7	LYS13, ARG14, HIS15 ARG21, ARG73, LYS96 LYS97	ARG5, ARG61, ARG68 ARG112, LYS116, ARG125 ARG128	LYS1, LYS33, ARG45 ARG114
9	LYS13, ARG14, HIS15 ARG21, ARG73, LYS96 LYS97, ARG128	ARG5, ARG61, ARG68 ARG112, LYS116, ARG125	LYS1, LYS33, ARG45 ARG114
11	LYS1, ARG5, LYS33 ARG45, ARG112, ARG114 LYS116, ARG125, ARG128	LYS13, ARG14, ARG61 ARG68	HIS15, ARG21, ARG73 LYS96, LYS97

for the pHs shown in Fig. 6.

Another feature we observe in Fig. 6 is that the increasing pH value promotes an orientational change of HEWL. Although the protein is adsorbed on the pore surface for the three pH values shown in Fig. 6 (see also the dark red circles in the Fig. 4A), we noticed an inversion between the residues belonging to Groups 1 and 3 caused by the increasing of pH towards HEWL's pI (pI ~ 11). Fig. 6D shows the side of the protein that is in contact with the pore in the two observed orientations at pH = 7 and 11 and $C_s = 0.001$ M. The arrows point out the location of the two closest residues to the pore surface. The protein surface is colored according to the ES potential and highlights the positive region (in blue) where these residues are located. Fig. 7 shows the probability distribution $\rho(r)$ of the six basic residues considered in Fig. 6, under the same conditions, except at pH = 10. In this case, $\rho(r)$ is bimodal since the protein changes its orientation with respect to the surface during the simulation. Snapshots of these two orientational states are shown in Figs. 7B and 7C.

Experimental investigations have demonstrated that the adsorption of HEWL is such that its short axis is perpendicular to the surface with N, C-terminus faces playing an important role (side-on orientation)[22,76–78]. In a series of studies using detailed atomistic Molecular Dynamics simulations, Kubiak-Ossowska and coauthors have focused on the adsorption of HEWL on flat charged silica surfaces at pH = 7[42,79–81]. They have found that ES interactions play a key role in guiding HEWL to the most favorable orientation with N, C-terminal face against the silica surface. Besides that, they have listed a set of residues – such as LYS1, ARG5, LYS13, ARG14, ARG125, and ARG128 – that are important for protein–surface anchoring. Yu and Zhou have studied the curvature effect of silica nanoparticles on the Lysozyme orientation and conformation by Molecular Dynamics simulations of a mesoscopic coarse-grained model at neutral pH[33]. They have verified that the number of binding sites increases with increasing nanoparticle curvature and decreasing salt concentration. Four of the seven residues belonging to Group 1 at pH = 7 in our results are the same as those mentioned by these works. This difference can be attributed to the charge regulation effects in our work, whereas the studies cited above[33,42,79–81] consider the residues with fixed pH independent charge. Recently, Boubeta and coauthors have proposed a theoretical framework to study the interaction between the Lysozyme and charged flat surfaces at pH = pI, taking into account charge–regulation effects[34]. They have found that LYS1, ARG5, LYS33, ARG114, ARG125 and ARG128 are much closer to the surface and likely more important for the protein-surface interaction. Our findings (see the bottom line in Table 2 and Fig. 6C) are not only in agreement with these results, but also with the experimental data from Dismer and colleagues who developed an effective lysine–labeling technique to identify possible binding orientations of Lysozyme on surfaces[78]. A change of the protein orientation at pH > 10 is also observed experimentally by Kubiak-Ossowska and coauthors but attributed to the dominance of hydrophobic forces[24]. In our case, we notice an orientational change even considering only electrostatic interactions.

Figures 8A-8C show the salt concentration effects on the probability distribution $\rho(r)$ of one residue of each Group defined above when the protein is within a pore of radius $a = 160$ Å at pH = 9. The increase in the salt concentration results in a decrease in the probability of ARG21 (Group 1) being near the pore surface. The same effect occurs for LYS33 (Group 3) be far from the pore surface. Furthermore, $\rho(r)$ presents a second peak for the residues belonging to Groups 1 and 3. The higher peak of the residue ARG21 (Group 1) corresponds approximately to the smaller peak of the residue LYS33 (Group 3) and vice versa. The residue ARG61, which belongs to Group 2, has a single peak at intermediary distances from the pore surface. As HEWL does not lose its native structure and its gyration radius remains constant, this behavior confirms the existence of two orientational states of the protein. Although the HEWL is adsorbed predominantly with residues from Group 1 in contact with the pore surface, the probability of the residues from Group 3 to be close to the surface is non-negligible as well. Nevertheless, the directionality of the adsorbed protein is getting lost with the increase of ionic strength due to screening of protein–surface ES interactions.

The pore radius effect can be seen in Figs. 8D-8F, which show the probability distribution $\rho(r)$ of residues ARG21, ARG61, and LYS33 for pore radius $a = 40$ Å (pink line), 80 Å (light red line), 120 Å (red line), and 160 Å (dark red line) at pH = 9 and 0.001 M of salinity. The reduction of the pore radius decreases the ES attraction between the protein and the surface. As already shown, the ES binding energy of adsorbed HEWL decreases (becomes less negative) with decreasing pore radius (see Fig. 4A and the discussion after it). The probabilities of the two orientations states approach each other with decreasing pore radius. In the smallest pore radius, $a = 40$ Å, we observed non-negligible probabilities of

Physical Chemistry Chemical Physics Accepted Manuscript

View Article Online
DOI: 10.1039/D1CP03185F

Published on 05 November 2021. Downloaded by Technical University of Munich on 11/5/2021 7:35:48 PM.

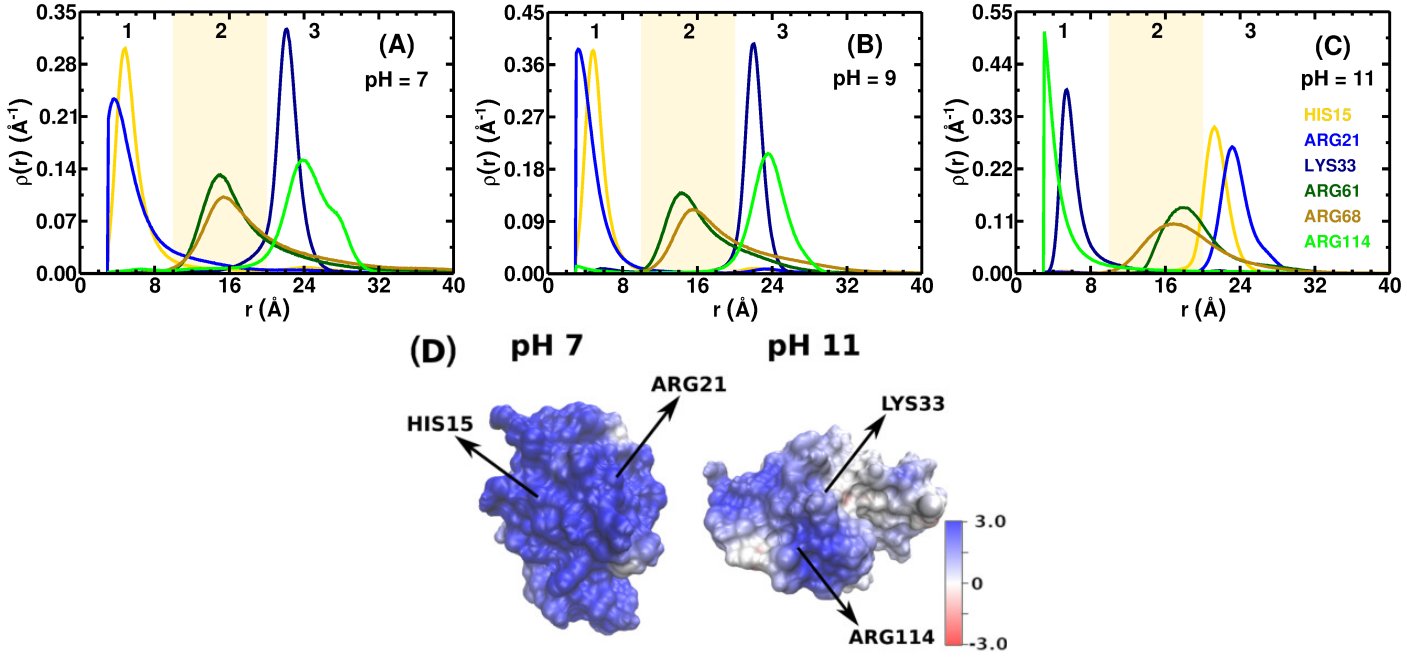

Fig. 6 Probability distribution of the residues HIS15 (yellow lines), ARG21 (blue lines), LYS33 (dark blue lines), ARG61 (dark green lines), ARG68 (dark yellow lines), and ARG114 (green lines) as a function of the distance r from the pore surface for three pHs: (A) pH $= 7$, (B) pH $= 9$, and (C) pH $= 11$. The pore radius is $a = 160$ Å and the salt concentration is 0.001 M. Regions 1, 2 and 3 correspond to the groups of basic residues which are more likely located at $r \leq 10$ Å (Group 1), $10\,\text{Å} < r \leq 20$ Å (Group 2), and $r > 20$ Å (Group 3), respectively, as detailed in Table 2. (D) ES potential at the HEWL surface calculated by means of APBS Electrostatic Extension of VMD [12,13] considering the mean charges obtained from our simulation at pH $= 7$ and 11 and salt concentration of 0.001 M. The negative potentials are shown in red and positive ones are in blue. The unit of electrostatic potential is k_BT/e ($\approx$ 25 mV)

.

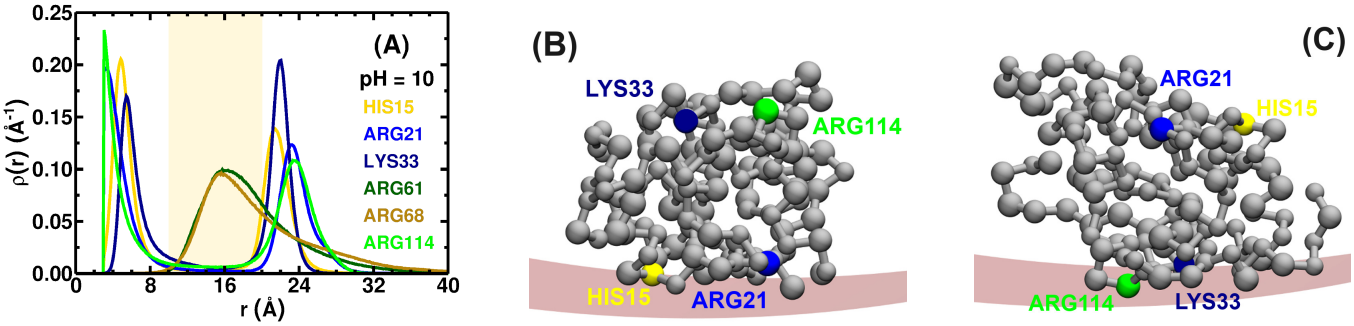

Fig. 7 Probability distribution of the residues HIS15 (yellow line), ARG21 (blue line), LYS33 (dark blue line), ARG61 (dark green line), ARG68 (dark yellow line), and ARG114 (green line) as a function of the distance r from the pore surface. The pore radius is $a = 160$ Å, the salt concentration is 0.001 M and pH $= 10$. The snapshots shown in (B) and (C) correspond to two orientational states of HEWL with the residues HIS15, ARG21, LYS33, and ARG114 highlighted in yellow, blue, dark blue and green, respectively.

Physical Chemistry Chemical Physics Accepted Manuscript

View Article Online
DOI: 10.1039/D1CP03185F

Published on 05 November 2021. Downloaded by Technical University of Munich on 11/5/2021 7:35:48 PM.

Physical Chemistry Chemical Physics Accepted Manuscript

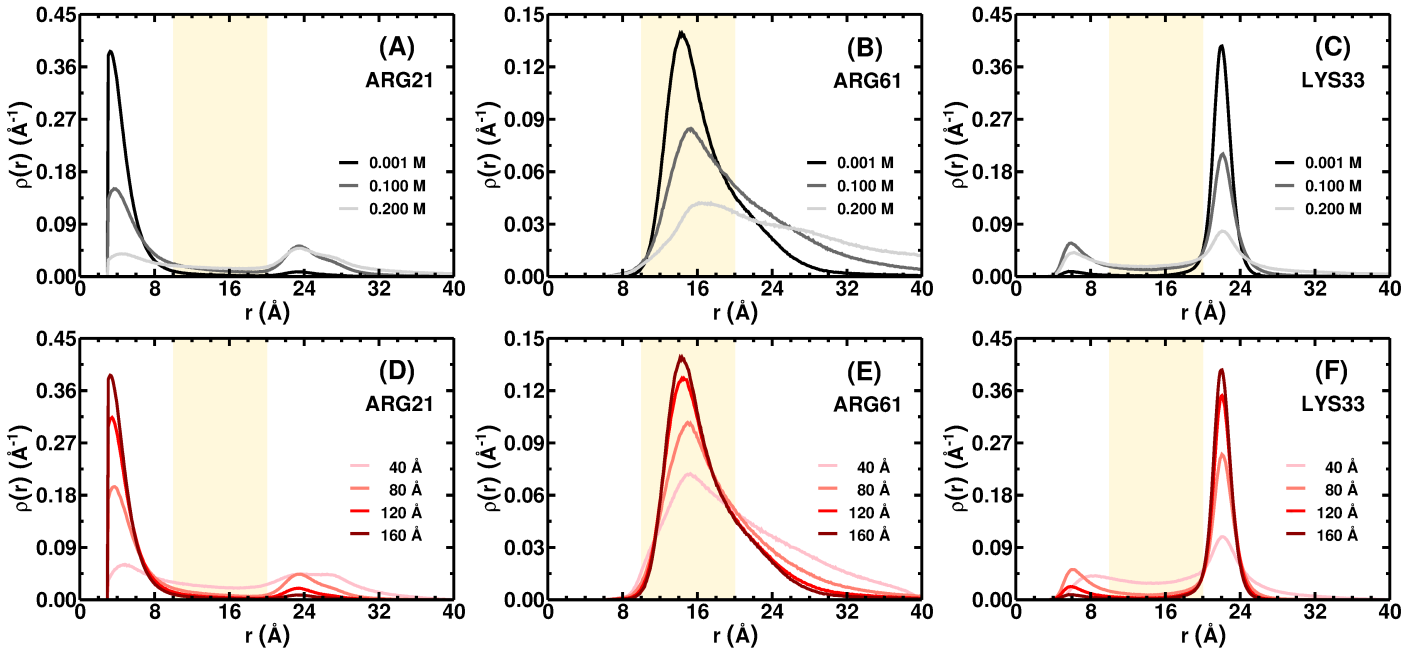

Fig. 8 Probability distribution of the residues ARG21 (graphs A and D), ARG61 (graphs B and E), and LYS33 (graphs C and F) as a function of the distance r from the pore surface. In the left column (graphs A, B, and C), we set the pore radius in $a = 160$ Å and vary the salt concentration: 0.001 M (black lines), 0.1 M (gray lines), and 0.200 M (light gray lines). In the right column (graphs D, E, and F), we set the salt concentration at 0.001 M and vary the pore radius: $a = 40$ Å (pink lines), $a = 80$ Å (light red lines), $a = 120$ Å (red lines), and $a = 160$ Å (dark red lines). In all graphs, we have pH = 9.

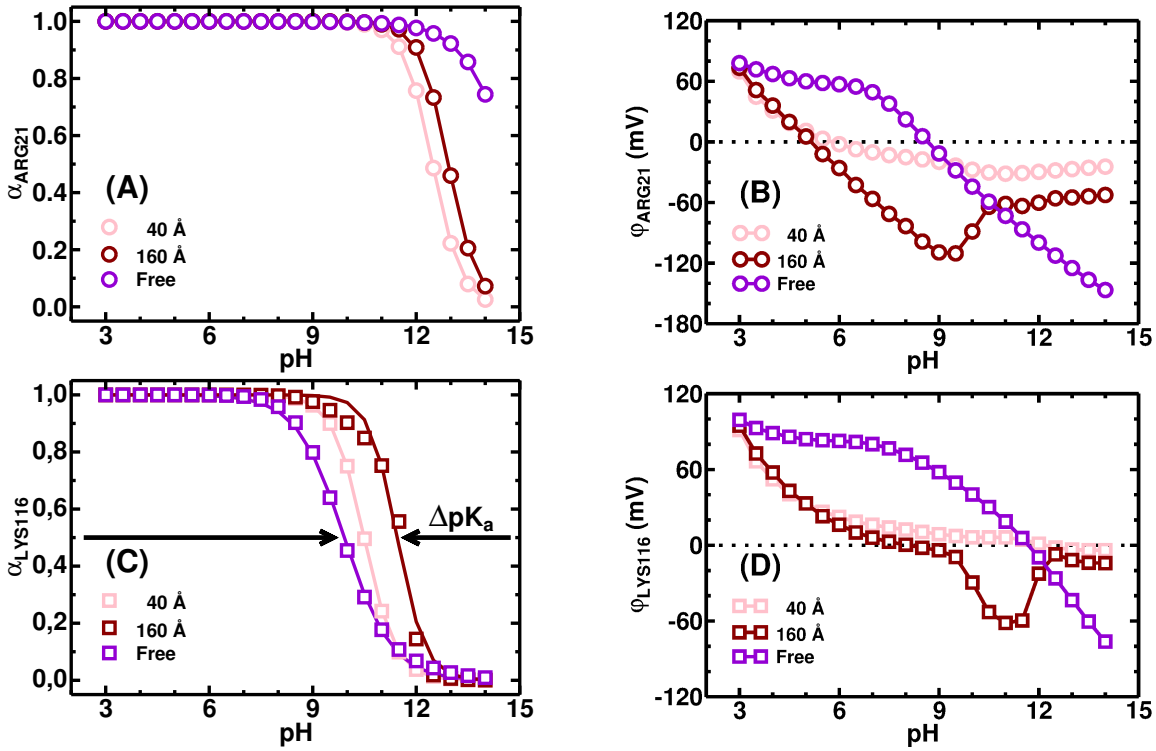

Fig. 9 Protonation degree, α, of the residues ARG21 (A) and LYS116 (C) in the presence (pink and dark red colors) and absence (purple color) of confinement. Empty circles and squares are the results from Monte Carlo simulation for the residues ARG21 and LYS116, respectively, whereas the lines represent the fits using the Hill equation (Eq. (7)). ES potential at the residues ARG21 (B) and LYS116 (D) in the presence (pink and dark red symbols) and absence (purple symbols) of confinement. In all cases, $C_s = 0.001$ M.

View Article Online
DOI: 10.1039/D1CP03185F

Published on 05 November 2021. Downloaded by Technical University of Munich on 11/5/2021 7:35:48 PM.

Table 3 The pK_a shift $\Delta pK_a = pK_a^{conf} - pK_a^{free}$ of basic residues from HEWL at low salt concentration (0.001 M).

Residues	ΔpK_a			
	$a = 160$ Å	$a = 120$ Å	$a = 80$ Å	$a = 40$ Å
LYS1	1.01 ± 0.02	0.73 ± 0.03	0.32 ± 0.02	-0.04 ± 0.02
ARG5	-0.95 ± 0.02	-1.04 ± 0.02	-1.14 ± 0.02	-1.25 ± 0.02
ARG14	-0.95 ± 0.02	-1.03 ± 0.02	-1.12 ± 0.02	-1.20 ± 0.02
HIS15	1.56 ± 0.02	1.34 ± 0.02	1.18 ± 0.02	1.14 ± 0.02
ARG21	-1.85 ± 0.02	-1.95 ± 0.02	-2.09 ± 0.02	-2.30 ± 0.02
LYS33	1.15 ± 0.03	0.86 ± 0.03	0.43 ± 0.02	0.04 ± 0.02
ARG45	-1.20 ± 0.02	-1.30 ± 0.02	-1.40 ± 0.02	-1.54 ± 0.02
ARG61	-0.99 ± 0.02	-1.08 ± 0.02	-1.16 ± 0.02	-1.25 ± 0.02
LYS116	1.55 ± 0.06	1.18 ± 0.05	0.82 ± 0.03	0.57 ± 0.03

the residues being at intermediate positions between two peaks, indicating the loss of directionality of the adsorbed protein.

We also verify how the adsorption of HEWL on a charged confining surface modify the pK_a of protein residues. To achieve this goal, the protonation degree α of each ionizable residue was calculated at several pH conditions for the free protein in solution and when confined in a pore. The pK_a was then obtained by fitting the individual titration curves using the Hill equation [82–85]

$$\alpha = \frac{1}{1 + 10^{\pm n(pH - pK_a)}}, \tag{7}$$

where the plus and minus signs are used for basic and acidic residues, respectively, and n is the Hill coefficient. This parameter provides information about the effect of the correlation between the residues in the course of the protonation. A Hill coefficient $n > 1$ means that the protonation is cooperative, i.e., the protonation of one residue is favored by the protonation of other ones, whereas if $n < 1$, the proton binding is anti-cooperative. In the case of $n = 1$, the residues behave independently of the others regarding the propensity towards protonation. In this work, for the HEWL free in solution, $n < 1$ for all titratable residues. As the protein is within the pore, $n > 1$ for the residues from Group 1 showed in Table 2 for pH = 11 (see Tables S1 and S2 in Supplementary Information). At this pH regime, the LYS and ARG residues are more susceptible to the charge–regulation effects since $pH \approx pK_a^{free}$, where the label "free" refers to the free protein in the solution. The protonation of one of these residues can cause variations in the strength and characteristics of adsorption that increases the ES potential effect on another one. The Hill coefficient approaches 1 with increasing ionic strength and decreasing pore radius due to the decreasing ES potential.

Table 3 shows the pK_a shift $\Delta pK_a = pK_a^{conf} - pK_a^{free}$ of HEWL residues at $C_s = 0.001$ M that have $|\Delta pK_a| > 1.0$ [47,48], where the label "conf" refers to the confined protein. The action of the ES potential of the pore surface on the ionizable residues changes their probability of protonation. Another equivalent way of looking at this situation, adopted in Ref. [86], is that surface ES potential changes de local pH which, in turn, affects the protonation degree of the ionizable residues when the protein is close to the surface. Furthermore, we verified that the reduction of the pore radius decreases $|E_B|$ and, consequently, the modulus of the ES potential (see Fig. 4A). As we can see in Table 3, lysine and histidine residues have a more pronounced pK_a shift for $a = 160$ Å, while arginine residues show a greater change in their pK_a in the smallest pore radius ($a = 40$ Å). The increase of the ES screening at 0.1 M of salt led to $|\Delta pK_a| < 1.0$ for all titratable residues and confinement conditions studied in this work.

In order to understand the inverse behavior of arginine residues with respect to change of their pK_a with the pore radius, Fig. 9A shows the degree of protonation α_{ARG21} of ARG21 residue for the HEWL free in the solution (purple color) and within the pore with radius $a = 40$ Å and 160 Å (pink and dark red colors, respectively) at $C_s = 0.001$ M. The protonation degree of ARG21, at pH $\geq$ 11 is as larger as the ES potential φ_{ARG21} acting on this residue is negative (see Fig. 9B). For pH > 12, the $|\varphi_{ARG21}|$ regarding the free protein in solution becomes larger, promoting the protonation of ARG21. The sensitivity of the protonation state to the action of the electrical potential from the pore surface is larger for $pH \approx pK_a^{free}$. In the case of ARG21, $pK_a^{free} = 14.78 \pm 0.01$ and the inversion of the ES potential behaviour in which φ_{ARG21} regarding the protein free in solution becomes more negative occurs for pH > 11. In the case of LYS116 (see Figs. 9C and 9D), which presents the highest positive ΔpK_a, this inversion of behaviour occurs at $pH \approx 12.5$ and $pK_a^{free} = 9.92 \pm 0.02$. As a consequence, the protonation process of LYS116 is favored when the HEWL is confined to a pore with radius $a = 160$ Å.

This pK_a shift causes a change in the protein charge distribution and its net charge, as shown in Table 4 for pore radius $a = 160$ Å, low ionic strength (0.001 M), and pH = 7 and 11. At pH = 7, far from the HEWL isoelectric point, the changes of the ES potential on the protein surface in contact with the pore surface are small; the same is observed for the protein net charge. Conversely, close to the isoelectric point of the protein, at pH = 11, the net charge grows about six times. The ES potential on the charge patch that contains the residues LYS33 and ARG114 also changes in this same proportion. This local induced charge density stabilizes the protein adsorption with the features shown in Fig. 6C. The evaluation of the multipole moments could also provide valuable informations about how the orientation depends on the protonation. As shown in Ref. [87], the charge regulation mechanism mixes the different protein multipole moments. This occurs because the protonation degree of each residue is affected by the charge density of the whole protein. Therefore, the action of the ES potential of the pore surface on the several ionizable residues

Physical Chemistry Chemical Physics Accepted Manuscript

View Article Online
DOI: 10.1039/D1CP03185F

Published on 05 November 2021. Downloaded by Technical University of Munich on 11/5/2021 7:35:48 PM.

Table 4 The net charge and ES potential at the HEWL surface calculated by means of APBS Electrostatic Extension of VMD[12,13] considering the mean charges obtained from our simulation at pH = 7 and 11 and $C_s = 0.001$ M. The negative potentials are shown in red and positive ones are in blue. The color scale is the same as in Fig. 6

	ES potential at the HEWL surface		Net charge	
pH	In solution	$a = 160$ Å	In solution	$a = 160$ Å
7	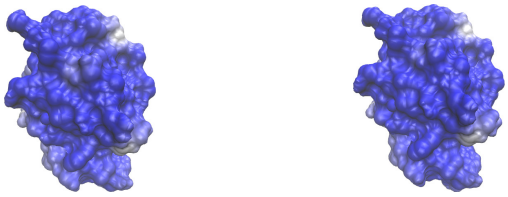		7.76	8.24
11	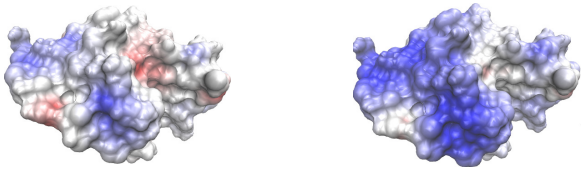		0.51	3.35

is self-consistently coupled with each other.

This is consistent with results by Narambuena and coauthors who have studied the adsorption of lysozyme on weak polyacid hidrogel films using a molecular theory[88]. They have verified that lysozyme adsorption occurs even under conditions where pH > pI due to charge–regulation effects. For example, they showed that, at pH = 11.3, the charge of the protein is approximately $-2e_0$ when it is in bulk solution and, when the Lysozyme is adsorbed, its charge increases up to approximately $+7e_0$.

4 Conclusions

In this study, we investigated the adsorption of hen egg-white lysozyme (HEWL) onto a negatively charged confining silica pore by means of constant-pH Monte Carlo simulations. We found that, except for the smallest pore radius, the protein-pore binding energy presents a minimum near HEWL's isoelectric point, suggesting that charge patches and the charge regulation process play an important role for adsorption, see Fig. 4. We identified that the HEWL adsorbs in two orientations dependent on pH. At neutral pH, the HIS15 and ARG21 are the residues closer to the pore surface. Increasing the pH towards the pI, the orientation changes with the residue ARG114 having an important role for the adsorption stability, see Fig. 6 and 7. In addition, as shown in Tables 2-4, we group the residues most likely to be close to the pore surface and found the protonation degree of these residues is significantly affected by the protein–pore ES interactions, thereby favoring protein adsorption. Extensions of the current study include the adsorption at different protein concentrations, which will enable us to evaluate the cooperative effects caused by protein–protein interactions and, accordingly, the factors determining the maximum loading inside the pore. As pointed out by Moerz and Huber[21], the presence of charged patches and charge regulation effects can be important for the adsorption of Cytochrome C and Myoglobin into SBA-15 mesoporous silica materials, where the maximum pore loading is observed at pH values below the isoelectric point.

The results presented in this study provide valuable information on the adsorption of proteins on charged materials and can be applied to a wider range of problems. Even adopting a simplified model for the protein, we obtained a good agreement with results from more detailed models and from experiments. An immediate application of our results includes the problems of protein adsorption in porous media. The maximum load within the charged pores is strongly dependent on protein–protein interaction and conditions on its net charge. Besides, the detailed protein charge distribution determines the orientation regarding the pore surface and of each protein with each other. These protein properties should be known when the protein is inside a pore and, as is shown by the results presented in this work, the changes of the protein properties regarding the protein free in the solution can be significant. This charge–regulation mechanism promotes not only a significant protein net charge at pH values close to the isoelectric point, that enhance the HEWL–silica adsorption, but also the distribution and charge density of charge patches on the protein surface, that determines the protein orientation regarding the pore surface. Here, returning to the idea of protein and drug delivery into a biological cell by nanoparticles of mesoporous silica, we emphasize that the shifts of pK_a for the protein residues found for HEWL in small pores should be tested for other proteins and ubiquitously used drug molecules. The shifts of pK_a for particular residues, depending on the pore dimensions and the pH level of the solution, can potentially present a mechanism for release of the drug molecules inside the target cancer cells (which typically feature smaller pH values than healthy tissues/cells).

Another possible application includes the adsorption of lytic peptides onto anionic lipid membrane. Recently, it was shown that the lipid ES potential and the solution pH affect the degree of protonation of peptides residues and modulates the affinity to the membrane[89]. It is known that at a given critical concentra-

Physical Chemistry Chemical Physics Accepted Manuscript

View Article Online
DOI: 10.1039/D1CP03185F

Published on 05 November 2021. Downloaded by Technical University of Munich on 11/5/2021 7:35:48 PM.

tion, these peptides form pores in the bilayer that leads to the cell–death of bacteria. Therefore, to know the peptides' charge distribution inside these charged confined enviroments should be essential to evaluate the driving forces and mechanisms of pore formation.

Conflicts of interest

There are no conflicts to declare.

Acknowledgements

All simulations were performed by resources supplied by the Center for Scientific Computing (NCC/GridUNESP) of the Sao Paulo State University (UNESP). Daniel L. Z. Caetano thanks the Sao Paulo Research Foundation (FAPESP, Grant No. 2013/08293-7 and 2019/19662-0) and the Coordenação de Aperfeiçoamento de Pessoal de Nível Superior, Brasil (CAPES), Finance Code 001 for the financial support. Ralf Metzler acknowledges support from the Foundation for Polish Science (FNP) within an Alexander von Humboldt Honorary Polish Research Scholarship. Sidney J. de Carvalho thanks to Sao Paulo Research Foundation (FAPESP, Process Grant No 2018/01841-2) for the financial support.

Notes and references

1 Z. Tao, *RSC Adv.*, 2014, **4**, 18961–18980.
2 P. Huber, *J. Phys.: Condens. Matter*, 2015, **27**, 103102.
3 M. Hartmann, *Chem. Mater.*, 2005, **17**, 4577–4593.
4 C. Ispas, I. Sokolov and S. Andreescu, *Anal. Bioanal. Chem.*, 2009, **393**, 543–554.
5 J. Lu, M. Liong, J. I. Zink and F. Tamanoi, *Small*, 2007, **3**, 1341–1346.
6 T. Xia, M. Kovochich, M. Liong, H. Meng, S. Kabehie, S. George, J. I. Zink and A. E. Nel, *ACS Nano*, 2009, **3**, 3273–3286.
7 R. Ravindra, S. Zhao, H. Gies and R. Winter, *J. Am. Chem. Soc.*, 2004, **126**, 12224–12225.
8 M. S. Cheung and D. Thirumalai, *J. Mol. Biol.*, 2006, **357**, 632–643.
9 A. Sirur, M. Knott and R. B. Best, *Phys. Chem. Chem. Phys.*, 2014, **16**, 6358–6366.
10 A. Calvo, B. Yameen, F. J. Williams, G. J. Soler-Illia and O. Azzaroni, *J. Am. Chem. Soc.*, 2009, **131**, 10866–10868.
11 V. V. Palyulin, T. Ala-Nissila and R. Metzler, *Soft Matter*, 2014, **10**, 9016–9037.
12 W. Humphrey, A. Dalke and K. Schulten, *J. Molec. Graphics*, 1996, **14**, 33–38.
13 N. Baker, D. Sept, S. Joseph, M. Holst and J. McCammon, *Proc. Natl. Acad. Sci. USA*, 2001, **98**, 10037–10041.
14 C. D. Cooper, N. C. Clementi and L. A. Barba, *J. Chem. Phys.*, 2015, **143**, 124709.
15 L.-C. Sang and M.-O. Coppens, *Phys. Chem. Chem. Phys.*, 2011, **13**, 6689–6698.
16 D. I. Fried, F. J. Brieler and M. Froeba, *ChemCatChem*, 2013, **5**, 862–884.
17 K. El-Boubbou, D. A. Schofield and C. C. Landry, *J. Phys. Chem. C*, 2012, **116**, 17501–17506.
18 A. Vinu, V. Murugesan and M. Hartmann, *J. Phys. Chem. B*, 2004, **108**, 7323–7330.
19 V. Steri, M. Monduzzi and A. Salis, *Microporous Mesoporous Mater.*, 2013, **170**, 164–172.
20 S. T. Moerz and P. Huber, *Langmuir*, 2014, **30**, 2729–2737.
21 S. T. Moerz and P. Huber, *J. Phys. Chem. C*, 2015, **119**, 27072–27079.
22 M. Rabe, D. Verdes and S. Seeger, *Adv. Colloid Interface Sci.*, 2011, **162**, 87–106.
23 A. D. Fernández, P. Charchar, A. G. Cherstvy, R. Metzler and M. W. Finnis, *Phys. Chem. Chem. Phys.*, 2020, **22**, 27955–27965.
24 K. Kubiak-Ossowska, M. Cwieka, A. Kaczynska, B. Jachimska and P. A. Mulheran, *Phys. Chem. Chem. Phys.*, 2015, **17**, 24070–24077.
25 N. Hildebrand, S. Köppen, L. Derr, K. Li, M. Koleini, K. Rezwan and L. Colombi Ciacchi, *J. Phys. Chem. C*, 2015, **119**, 7295–7307.
26 J. Zhou, J. Zheng and S. Jiang, *J. Phys. Chem. B*, 2004, **108**, 17418–17424.
27 Y. Xie, W. Gong, J. Jin, Z. Zhao, Z. Li and J. Zhou, *Appl. Surf. Sci.*, 2020, **506**, 144962.
28 J. Liu, G. Yu and J. Zhou, *Chem. Eng. Sci.*, 2015, **121**, 331–339.
29 T. Hagiwara, T. Sakiyama and H. Watanabe, *Langmuir*, 2008, **25**, 226–234.
30 F. Carlsson, E. Hyltner, T. Arnebrant, M. Malmsten and P. Linse, *J. Phys. Chem. B*, 2004, **108**, 9871–9881.
31 Y. Xie, J. Zhou and S. Jiang, *J. Chem. Phys.*, 2010, **132**, 02B602.
32 G. Yu, J. Liu and J. Zhou, *J. Phys. Chem. B*, 2014, **118**, 4451–4460.
33 G. Yu and J. Zhou, *Phys. Chem. Chem. Phys.*, 2016, **18**, 23500–23507.
34 F. Boubeta, G. Soler-Illia and M. Tagliazucchi, *Langmuir*, 2018, **34**, 15727–15738.
35 A. G. Cherstvy and R. G. Winkler, *J. Phys. Chem. B*, 2012, **116**, 9838–9845.
36 C. H. Evers, T. Andersson, M. Lund and M. Skepö, *Langmuir*, 2012, **28**, 11843–11849.
37 J. Henriques and M. Skepö, *Food Hydrocolloids*, 2015, **43**, 473–480.
38 M. Lund, T. Åkesson and B. Jönsson, *Langmuir*, 2005, **21**, 8385–8388.
39 M. Lund and B. Jönsson, *Q. Rev. Biophys.*, 2013, **46**, 265–281.
40 F. L. Barroso da Silva, M. Lund, B. Jönsson and T. Åkesson, *J. Phys. Chem. B*, 2006, **110**, 4459–4464.
41 F. L. Barroso da Silva, M. Boström and C. Persson, *Langmuir*, 2014, **30**, 4078–4083.
42 K. Kubiak and P. A. Mulheran, *J. Phys. Chem. B*, 2009, **113**, 12189–12200.
43 G. Borgohain and S. Paul, *J. Mol. Liq.*, 2017, **233**, 431–441.
44 K. Kubiak-Ossowska, B. Jachimska, M. Al Qaraghuli and P. A.

Physical Chemistry Chemical Physics Accepted Manuscript

View Article Online
DOI: 10.1039/D1CP03185F

Published on 05 November 2021. Downloaded by Technical University of Munich on 11/5/2021 7:35:48 PM.

Mulheran, *Curr. Opin. Colloid Interface Sci.*, 2019, **41**, 104–117.
45 S. Hikima, J.-i. Hikima, J. Rojtinnakorn, I. Hirono and T. Aoki, *Gene*, 2003, **316**, 187–195.
46 R. Cegielska-Radziejewska, G. Lesnierowski and J. Kijowski, *Pol. J. Food Nutr. Sci.*, 2008, **58**, 5–10.
47 V. G. Contessoto, V. M. De Oliveira, S. J. De Carvalho, L. C. Oliveira and V. B. Leite, *J. Chem. Theory Comput.*, 2016, **12**, 3270–3277.
48 V. M. de Oliveira, V. de Godoi Contessoto, F. B. da Silva, D. L. Z. Caetano, S. J. de Carvalho and V. B. P. Leite, *Biophys. J.*, 2018, **114**, 65–75.
49 C. Clementi, H. Nymeyer and J. N. Onuchic, *J. Mol. Biol.*, 2000, **298**, 937–953.
50 N. Koga and S. Takada, *J. Mol. Biol.*, 2001, **313**, 171–180.
51 H. Lammert, A. Schug and J. N. Onuchic, *Proteins: Struct., Funct., Bioinf.*, 2009, **77**, 881–891.
52 J. K. Noel, P. C. Whitford, K. Y. Sanbonmatsu and J. . N. Onuchic, *Nucleic Acids Res.*, 2010, **38**, W657–W661.
53 V. G. Contessoto, D. T. Lima, R. J. Oliveira, A. T. Bruni, J. Chahine and V. B. Leite, *Proteins: Struct., Funct., Bioinf.*, 2013, **81**, 1727–1737.
54 V. M. de Oliveira, D. L. Z. Caetano, F. B. da Silva, P. R. Mouro, A. B. de Oliveira Jr, S. J. de Carvalho and V. B. Leite, *J. Chem. Theory Comput.*, 2020, **16**, 765–772.
55 V. Sobolev, A. Sorokine, J. Prilusky, E. E. Abola and M. Edelman, *Bioinformatics*, 1999, **15**, 327–332.
56 S. Kumar, J. Rosenberg, D. Bouzida, R. Swendsen and P. Kollman, *J. Comput. Chem.*, 1995, **16**, 1339–1350.
57 J. K. Noel, M. Levi, M. Raghunathan, H. Lammert, R. L. Hayes, J. N. Onuchic and P. C. Whitford, *PLoS computational biology*, 2016, **12**, e1004794.
58 S. Venkataramani, J. Truntzer and D. R. Coleman, *J. Pharm. Bioallied Sci.*, 2013, **5**, 148.
59 M. A. Brown, A. Goel and Z. Abbas, *Angew. Chem., Int. Ed. Engl.*, 2016, **55**, 3790–3794.
60 S. J. de Carvalho, R. Metzler and A. G. Cherstvy, *Soft Matter*, 2015, **11**, 4430–4443.
61 A. G. Cherstvy, *Biopolymers*, 2012, **97**, 311–317.
62 S. de Carvalho, R. Ghiotto and F. da Silva, *J. Phys. Chem. B*, 2006, **110**, 8832–8839.
63 K. Binder, *Monte Carlo and molecular dynamics simulations in polymer science*, Oxford University Press, 1995.
64 C. E. Reed and W. F. Reed, *J. Chem. Phys.*, 1992, **96**, 1609–1620.
65 A. G. Cherstvy, *J. Phys. Chem. B*, 2009, **113**, 4242–4247.
66 D. Srivastava, E. Santiso, K. Gubbins and F. L. Barroso da Silva, *Langmuir*, 2017, **33**, 11417–11428.
67 F. L. Barroso da Silva and L. G. Dias, *Biophys. Rev.*, 2017, **9**, 699–728.
68 C. A. Haynes, E. Sliwinsky and W. Norde, *J. Colloid Interface Sci.*, 1994, **164**, 394–409.
69 T. Curk and E. Luijten, *Phys. Rev. Lett.*, 2021, **126**, 138003.
70 J. Landsgesell, P. Hebbeker, O. Rud, R. Lunkad, P. Kosovan and C. Holm, *Macromolecules*, 2020, **53**, 3007–3020.
71 F. Grünewald, P. C. T. Souza, H. Abdizadeh, J. Barnoud, de Vries Alex H. and S. J. Marrink, *J. Chem. Phys.*, 2020, **153**, 024118.
72 Y. Abe, T. Ueda, H. Iwashita, Y. Hashimoto, H. Motoshima, Y. Tanaka and T. Imoto, *J. Biochem.*, 1995, **118**, 946–952.
73 G. B. Goh, B. S. Hulbert, H. Zhou and C. L. Brooks III, *Proteins: Struct., Funct., Genet.*, 2014, **82**, 1319–1331.
74 W. Krigbaum and F. Kügler, *Biochemistry*, 1970, **9**, 1216–1223.
75 F. Felsovalyi, P. Mangiagalli, C. Bureau, S. K. Kumar and S. Banta, *Langmuir*, 2011, **27**, 11873–11882.
76 T. J. Su, J. R. Lu, R. K. Thomas, Z. F. Cui and J. Penfold, *J. Colloid Interface Sci.*, 1998, **203**, 419–429.
77 K. Nakanishi, T. Sakiyama and K. Imamura, *J. Biosci. Bioeng.*, 2001, **91**, 233–244.
78 F. Dismer, M. Petzold and J. Hubbuch, *J. Chromatogr. A*, 2008, **1194**, 11–21.
79 K. Kubiak-Ossowska and P. A. Mulheran, *Langmuir*, 2010, **26**, 15954–15965.
80 K. Kubiak-Ossowska and P. A. Mulheran, *Langmuir*, 2010, **26**, 7690–7694.
81 K. Kubiak-Ossowska and P. A. Mulheran, *Langmuir*, 2012, **28**, 15577–15585.
82 C. R. Cantor and P. R. Schimmel, *Biophysical chemistry: Part III: the behavior of biological macromolecules*, Macmillan, 1980.
83 A. Onufriev, D. A. Case and G. M. Ullmann, *Biochemistry*, 2001, **40**, 3413–3419.
84 R. E. Georgescu, E. G. Alexov and M. R. Gunner, *Biophys. J.*, 2002, **83**, 1731–1748.
85 M. S. Lee, F. R. Salsbury Jr and C. L. Brooks III, *Proteins: Struct., Funct., Bioinf.*, 2004, **56**, 738–752.
86 R. J. Nap, A. L. Bozic, I. Igal Szleifer and R. Podgornik, *Biophys. J.*, 2014, **107**, 1970–1979.
87 A. L. Bozic and R. Podgornik, *J. Chem. Phys.*, 2018, **149**, 163307.
88 C. F. Narambuena, G. S. Longo and I. Szleifer, *Soft Matter*, 2015, **11**, 6669–6679.
89 D. Alvares, I. Martins, T. Viegas, M. Palma, A. Araujo, S. de Carvalho and J. Ruggiero Neto, *Membranes*, 2021, **11**, 307.

Physical Chemistry Chemical Physics Accepted Manuscript